Simulation of Supersonic Reacting Hydrocarbon Flows with Detailed Chemistry

*Scott G. Sheffer**, *Luigi Martinelli*†, *and Antony Jameson*‡
CFD Laboratory for Engineering Analysis and Design
Department of Mechanical and Aerospace Engineering
Princeton University
Princeton, New Jersey 08544 U.S.A.

Abstract

This paper presents a parallel multigrid method for computing inviscid and viscous high speed steady-state flows with reacting hydrocarbons. The governing equations for reactive flow are solved using an explicit multigrid algorithm while treating the chemical source terms in a point implicit manner. The CUSP (Convective Upwind and Split Pressure) scheme is used to provide necessary artificial dissipation without contaminating the solution. This explicit method yields excellent parallel speedups, thus enabling the calculation of reactive flows with detailed chemical kinetics including large numbers of species and reactions. Results indicate good multigrid speedups and adequate resolution of the reaction zone in inviscid and viscous two-dimensional hydrogen/air and methane/air test cases.

Nomenclature

$\mathbf{C}(\mathbf{w}_{ij})$	convective Euler fluxes
$\mathbf{D}(\mathbf{w}_{ij})$	diffusive and dissipative fluxes
D_i	diffusion coefficient for species i
D_{ij}	binary diffusion coefficient between species i and j
E	total energy (internal, chemical and kinetic)
$\mathbf{f}, \mathbf{g}$	convective flux vectors
$\mathbf{f_v}, \mathbf{g_v}$	diffusive flux vectors
h_i	static enthalpy of species i
M	Mach number
p	static pressure
$\mathbf{q}$	conductive heat flux vector
R	mixture gas constant
$\mathcal{R}$	universal gas constant
$\mathbf{R}(\mathbf{w}_{ij})$	total flux residual for cell i,j
T	static temperature
u, v	Cartesian velocity components
u_{di}, v_{di}	diffusion velocity components for species i
V_{ij}	volume of cell i,j
$\mathbf{w}$	vector of flow variables
X_i	mole fraction of species i
γ	mixture ratio of specific heats
ρ	density
ρ_i	density of species i
$\dot{\omega}$	chemical source term
$\Omega, \partial\Omega$	cell element and boundary

* Graduate Student, Student Member AIAA

†Assistant Professor of Aerospace Engineering, AIAA Member

‡James S. McDonnell Distinguished University Professor of Aerospace Engineering, AIAA Fellow

Introduction

The simulation of high speed chemically reacting flows is a very challenging area for computational efforts. The presence of shock waves necessitates good shock capturing properties, while chemical reactions require avoiding excessive numerical dissipation so that the solution remains uncontaminated. Viscous effects, heat conduction and species diffusion complicate reactive flow calculations, both from the increased computational work required and because of possible interactions between the chemistry and these effects. Diffusion of radical species in a boundary layer may significantly alter the resulting flowfield. Exponential increases and decreases of radical species in small spatial zones lead to large gradients that must simultaneously be captured without oscillation and without unnecessary dissipation. In addition, the stiff nature of the chemical source terms and the additional species conservation equations make the integration of the governing equations very difficult and time consuming.

The inherent inaccuracy of chemical rate data presents another challenge to modeling reactive flows. The turn around time of reactive flow simulations must be made short enough so that varying rate coefficients may be examined to determine which set is the most appropriate for modeling a particular phenomena.

Because most chemical reactions have characteristic times much less than those of the convective flow field, many explicit schemes are handicapped in computing such flows. The time step for an explicit scheme is proportional to the shortest characteristic time, so that stability restrictions require very short time steps in reactive flow simulations. This short time step leads to very long simulation times for steady state computations.

Several ways to overcome this limitation of explicit schemes have been explored. The first is to use a fully implicit scheme for the steady state computation, thus removing stability limitations completely. Wilson and MacCormack [19] used such a scheme to compute hydrogen/air combustion over high speed blunt projectiles. Shuen and Yoon [15] used an LU-SSOR scheme to calculate pre-mixed and non-pre-mixed chemically reacting flow including viscous effects. Yungster [22] used an LU-SSOR scheme to compute shock-wave/boundary layer interactions in premixed combustible gas flows. Yungster and Rabinowitz [23] used the same scheme to simulate shock-induced methane/air combustion. Ju [7] implemented an LU-SGS scheme to calculate several reactive viscous flows. These implicit methods may accelerate convergence to steady state, but entail inverting large numbers of matrices and link the solution domain together in a way that may hamper parallelization. In addition, for unsteady simulations, the restriction on the time step for time accuracy may be the dominant factor, removing the advantage gained by the unconditional stability of the implicit scheme.

Another way of reducing the effect of the chemical term stiffness is to treat the source term in a point implicit manner. In this formulation due to Bussing and Murman [1], the source term at the next time level is linearized about the current time level, leading to a fully explicit equation at the cost of a matrix inversion. This action has the effect of preconditioning the species continuity equations, rescaling the chemical characteristic time so that it is of the same order as the convective characteristic time.

The fully explicit nature of the point implicit scheme allows the algorithm to be implemented in a fairly straightforward manner on a parallel computing platform. Because of the compact stencil used in the underlying explicit numerical discretization, the cost of parallel communication is quite low. This attribute, combined with the large amount of computational work involved for each cell in a reactive flow simulation, leads to a highly parallel efficient algorithm [12].

The use of multigrid acceleration for reactive flow calculations has not been adequately examined until recently. Multigrid techniques may have been thought to be too dissipative and cause radical species to be moved to physically incorrect regions. However, proper multigrid techniques [12, 13], in which the coarse grids are forced by the fine grid solution, can in fact be used to compute chemically reacting flows. Because of the large number of species and reactions involved in hydrocarbon combustion and the addition of viscous effects and species diffusion, a way to accelerate convergence is sorely needed. While parallelization will decrease the computational time associated with a numerical simulation, multigrid techniques represent an effective and efficient convergence acceleration tool for steady state reactive flow calculations.

In this work, the point-implicit formulation of Bussing and Murman is combined with an explicit time-stepping multigrid solver [10] using CUSP dissipation to compute high speed reactive flows. The fully explicit algorithm is parallelized using the MPI standard on an IBM SP-2 to achieve high parallel speedups.

Governing Equations

The two-dimensional equations for chemically reacting flow can be written in a Cartesian coordinate system (x, y) as:

$$\frac{\partial \mathbf{w}}{\partial t} + \frac{\partial (\mathbf{f} - \mathbf{f_v})}{\partial x} + \frac{\partial (\mathbf{g} - \mathbf{g_v})}{\partial y} = \dot{\omega}, \qquad (1)$$

where $\mathbf{w}$ is the vector of flow variables, $\mathbf{f}$ and $\mathbf{g}$ are the convective flux vectors, $\mathbf{f_v}$ and $\mathbf{g_v}$ are the diffusive flux vectors and $\dot{\omega}$ is the vector of source terms. Consider a control volume Ω with boundary $\partial\Omega$. The equations of motion of the fluid can then be written in integral form as

$$\frac{d}{dt}\iint_{\Omega} \mathbf{w}\, dx\, dy + \oint_{\partial\Omega} (\mathbf{f}\, dy - \mathbf{g}\, dx) = \oint_{\partial\Omega} (\mathbf{f_v}\, dy - \mathbf{g_v}\, dx) + \iint_{\Omega} \dot{\omega}\, dx\, dy, \qquad (2)$$

where $\mathbf{w}$ is the vector of flow variables

$$\mathbf{w} = \begin{Bmatrix} \rho_i \\ \rho u \\ \rho v \\ \rho E \end{Bmatrix},$$

$\mathbf{f}$, $\mathbf{g}$ are the convective flux vectors

$$\mathbf{f} = \begin{Bmatrix} \rho_i u \\ \rho u^2 + p \\ \rho uv \\ \rho E u + p u \end{Bmatrix}, \mathbf{g} = \begin{Bmatrix} \rho_i v \\ \rho uv \\ \rho v^2 + p \\ \rho E v + p v \end{Bmatrix},$$

$\mathbf{f_v}$, $\mathbf{g_v}$ are the diffusive flux vectors including species diffusion effects

$$\mathbf{f_v} = \begin{Bmatrix} -\rho_i u_{di} \\ \tau_{xx} \\ \tau_{xy} \\ -q_x - \sum_{i=1}^{N} \rho_i u_{di} h_i + \tau_{xx} u + \tau_{xy} v \end{Bmatrix},$$

$$\mathbf{g_v} = \begin{Bmatrix} -\rho_i v_{di} \\ \tau_{yx} \\ \tau_{yy} \\ -q_y - \sum_{i=1}^{N} \rho_i v_{di} h_i + \tau_{yx} u + \tau_{yy} v \end{Bmatrix},$$

and $\dot{\omega}$ is the chemical source vector

$$\dot{\omega} = \begin{Bmatrix} \dot{\omega}_i \\ 0 \\ 0 \\ 0 \end{Bmatrix}.$$

In these equations, $i = 1, \ldots, N$ and N is the number of species. For a thermally perfect gas, pressure may be determined from

$$p = \rho R T$$

where R is the mixture gas constant. The density is found from

$$\rho = \sum_{i=1}^{N} \rho_i.$$

Temperature may be determined from the following relation,

$$E = e + \frac{1}{2}\left(u^2 + v^2\right) = \sum_{i=1}^{N} \frac{\rho_i}{\rho} h_i - \frac{p}{\rho} + \frac{1}{2}\left(u^2 + v^2\right)$$

where h_i are the individual species enthalpies which depend solely on temperature for a thermally perfect gas. Combining the NASA polynomial representation of species enthalpies [4] with the previous equation for energy yields an implicit equation for temperature which is solved by Newton iteration.

As a first approximation, Fick's Law is used to determine the individual species diffusion velocities:

$$\rho_i \mathbf{u}_{di} = -\rho D_i \nabla\left(\frac{\rho_i}{\rho}\right).$$

The diffusion coefficient D_i is determined from the formulation following Williams [18] such that

$$D_i = \frac{1 - X_i}{\sum_{j \neq i} \frac{X_j}{D_{ij}}}$$

where X_i is the mole fraction of species i and D_{ij} is the binary diffusion coefficient between species i and j. The mixture viscosity and thermal conductivity are obtained in a mixture–averaged manner [8].

Chemical Model

Two different chemistry models are used in this paper. The hydrogen/oxygen chemistry model is that of Yetter *et al.* [21, 9, 20]. This mechanism, which is part of a broader mechanism for the $CO/H_2O/O_2$ system, contains eight reacting species and 21 reactions. The methane/air mechanism used in this work is taken from Yungster and Rabinowitz [23]. Using the technique of detailed reduction [17], they reduced mechanisms containing 28 to 50 species and 100 to 250 reactions down to a 19 reacting species, 52 reaction set. The model was validated by computing ignition delays and flame velocities that compared well with results from various shocktube experiments.

The chemical source terms are computed in the Arrhenius form, with the forward rate coefficients, k_{fj}, given by

$$k_{f_j} = A_j T^{n_j} \exp\left(\frac{-E_{Aj}}{\mathcal{R}T}\right) \tag{3}$$

where E_{Aj} is the activation energy of the jth forward reaction. Reactions that occur in the fall-off regime are also allowed for, following the formulation of Frenklach et al. [3]. The reverse rate coefficients are evaluated using the equilibrium constant for concentration

$$K_{c_j} = \frac{k_{f_j}}{k_{b_j}}. \tag{4}$$

This concentration equilibrium constant is obtained from the equilibrium constant in terms of partial pressures:

$$K_{c_j} = K_{p_j} \left(\frac{p_{atm}}{\mathcal{R}T}\right)^{\sum_{i=1}^{N} \nu_{ij}} \tag{5}$$

where N is the number of species and ν_{ij} is the change in the number of moles of species i in reaction j. The equilibrium constant K_{p_j} is calculated from the standard Gibbs free energy change for each reaction. Standard state free energies are obtained from the NASA polynomial set [4].

Numerical Model

Flow Equations

The governing equations are solved using a conservative explicit second-order accurate finite volume formulation in which the chemical source terms are treated point implicitly.

When the integral governing equations (2) are independently applied to each cell i, j in the domain, we

obtain a set of coupled ordinary differential equations of the form

$$\frac{d}{dt}(\mathbf{w}_{ij})V_{ij} + \mathbf{C}(\mathbf{w}_{ij}) + \mathbf{D}(\mathbf{w}_{ij}) = \dot{\omega}V_{ij}, \quad (6)$$

where $\mathbf{C}(\mathbf{w}_{ij})$ are the convective Euler fluxes, $\mathbf{D}(\mathbf{w}_{ij})$ includes the diffusive fluxes and the artificial dissipation fluxes added for numerical stability reasons and $\dot{\omega}V_{ij}$ are the chemical source terms. This equation (6) can be rewritten as follows (drop the i, j subscripts for clarity):

$$\frac{d}{dt}[\mathbf{w}]V + \mathbf{R}(\mathbf{w}) = \dot{\omega}V, \quad (7)$$

where $\mathbf{R}$ is the sum of the two flux contributions. The governing ordinary differential equations are solved using a standard five-stage time stepping scheme [11].

Chemical Source Terms

The chemical source vector $\dot{\omega}$ was treated in a point implicit manner [1]. An explicit treatment of the source terms leads, in general, to a time step restriction due to the stability limitation of the explicit scheme. This time step can be orders of magnitude less than the time step of the convective terms. Treating the source terms implicitly removes the stability criterion at the expense of a matrix inversion. The point implicit treatment reduces the stiffness of the problem by effectively rescaling the characteristic time of the reactions so that their magnitudes are commensurate with the convective characteristic time. We begin by writing the governing ordinary differential equation for cell i, j but instead evaluate the chemical source vector at the next time level:

$$\frac{d}{dt}[\mathbf{w}]V + \mathbf{R}(\mathbf{w}^n) = \dot{\omega}^{n+1}V. \quad (8)$$

We then linearize the chemical source vector about the present time level so that

$$\dot{\omega}^{n+1} \approx \dot{\omega}^n + \frac{\partial \dot{\omega}}{\partial \mathbf{w}}^n \frac{d}{dt}[\mathbf{w}]\Delta t. \quad (9)$$

Substituting this into the governing equation and rearranging yields

$$\frac{d}{dt}[\mathbf{w}]V = \left[\mathbf{I} - \Delta t \frac{\partial \dot{\omega}}{\partial \mathbf{w}}^n\right]^{-1} [\dot{\omega}^n V - \mathbf{R}(\mathbf{w}^n)], \quad (10)$$

which is evaluated entirely at the current time level and is thus fully explicit.

This treatment necessitates the inversion of the source term Jacobian matrix with dimension $N \times N$ where N is the number of species present in the flow. An inversion for the momentum and energy equations is not necessary due to the absence of chemical source terms in those equations. This $N \times N$ inversion is done only during the first stage of each time step of the solver and is retained and used for the succeeding four stages. This time-saving measure has no effect on the results of the computation.

Because the chemical source terms have been treated implicitly, the time step limitation of the explicit time integration scheme depends solely on the spectral radius of the flux Jacobian.

Numerical Dissipation

The Convective Upwind and Split Pressure (CUSP) scheme provides excellent resolution of shocks at high Mach numbers at a reasonable computational cost [5, 6]. The CUSP splitting is combined with a LED or ELED limiter to achieve second order accuracy in smooth regions with oscillation-free capture of shocks and large gradient regions. CUSP has been shown to be an accurate and effective dissipation scheme for viscous flows [16] and high speed reactive flows [14, 12, 13].

Boundary Conditions

The surface boundary is modeled as an adiabatic, non-catalytic surface. For Euler calculations, flow tangency is enforced at the surface while a no-slip boundary condition is used for viscous flows. Due to the supersonic nature of the flow, outflow boundary quantities are extrapolated from the interior and inflow quantities are taken to be free stream values.

Free stream values of radical species are set to a mass fraction of 1×10^{-11}. Varying this value did not affect the results.

Parallelization

The MPI standard is used to parallelize the code on an IBM SP-2. A static domain decomposition with two-level halos for flow quantities and one-level halos for grid information is used. The current point implicit scheme will achieve a higher level of speedup as compared to a convective flow code alone due to the greater number of operations that take place per cell [14, 12].

Multigrid Convergence Acceleration

Multigrid acceleration has been applied quite successfully to the solution of both the non-reactive Euler and Navier-Stokes equations [10, 11, 16]. How-

ever, the application of multigrid methods to reactive flow calculations has been limited. Bussing and Murman [1] reported success in using Ni's multigrid method for one-dimensional reactive flow calculations. Additional examples of multigrid acceleration for reactive flows are lacking.

The approach taken in this paper is to use a previously validated multigrid solver [10, 11, 16] and include chemical source terms on all levels [12, 13]. The coarse grid corrections to the species densities are limited to ensure that no mass fraction becomes negative. Varying degrees of underrelaxation can be used to enhance the convergence rate while capturing the sharp gradients and large radical growth regions that characterize reactive flow problems.

Results and Discussion

The formulation described in this paper was applied to inviscid two-dimensional flows over blunt bodies and two-dimensional viscous ramp flows. A two dimensional viscous reactive test case was taken from an experiment performed by Fielding [2]. In this experiment (Figure 1), a wedge of half angle 6.34° was placed in a free stream of partially reacted hydrogen and air. The object of the experiment was to see if radical–seeded hydrogen–air mixtures would react at low pressures over a wedge after passing through an oblique shock. The mass fractions of

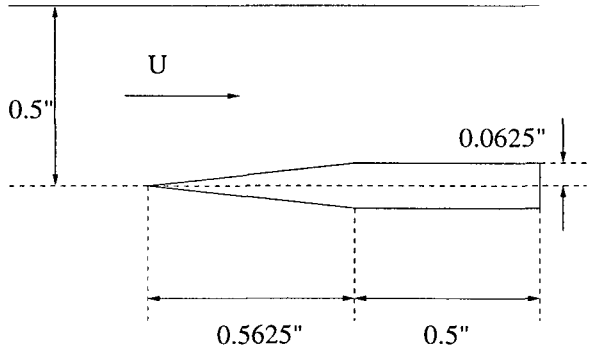

Figure 1: Experimental setup for viscous wedge.

the inlet flow were determined by Fielding using a one dimensional reacting gas code and are given in Table 1. Hydrogen had been injected into the air stream upstream of the ramp, partially reacted and then expanded so that the flow constituents became frozen. Species diffusion and heat conduction effects are included in the simulation. The nine species, 21 reaction model of Yetter *et al.* was used because it had been the model utilized to generate the composition of the incoming flow. In this model, it was assumed that nitrogen was an inert diluent. The flow was simulated on a grid with 128 cells in the streamwise direction and 96 in the direction normal

Species	Mass Fraction
H_2	6.86×10^{-3}
O_2	1.75×10^{-1}
H_2O	2.86×10^{-2}
N_2	7.84×10^{-1}
H	2.33×10^{-4}
O	9.66×10^{-4}
OH	1.65×10^{-4}
HO_2	3.97×10^{-3}
H_2O_2	4.76×10^{-10}

Table 1: Free stream mass fractions for hydrogen–air viscous wedge flow.

to the plate, with approximately 32 cells within the boundary layer.

In a previous paper [13], flow at a Mach number of 2.1 over the wedge had been simulated. In order to provide greater understanding of the physical processes in this flow, two additional simulations have been performed. Due to the lack of reaction in the previous $M = 2.1$ case, the free stream Mach number was increased to $M = 2.92$. This higher Mach number causes an increase in the temperature in the boundary layer of the flow, which could increase the Damköhler number in that region to the point where strong reaction might take place. The pressure was lowered to a value of 0.0157 atmospheres to match a one-dimensional prediction of Fielding [2]. The temperature in the free stream flow was changed to approximately 440 K, again to match a one-dimensional prediction.

This $M = 2.92$ flow is shown in Figures 2 and 3. Density contours are depicted in Figure 2 which shows a relatively thick boundary layer. The oblique shock angle is 25.9° while the exact analytic value for this Mach number and wedge angle pair is 24.5°. This difference may be explained by reactions due to the nonequilibrium nature of the inlet flow at this free stream pressure and temperature which cause the Mach number to decrease in the streamwise direction. Figure 3 shows the logarithm of the mass fraction of OH. Again, similar to the case presented previously, little reaction progress is seen, with some OH forming water vapor at the end of the ramp near the exit plane. The maximum mass fraction of water is approximately 4%. In this case, the flow apparently has a rather low Damköhler number due to the low pressure and temperature in the boundary layer.

The free stream Mach number was then increased to $M = 4.0$ and the free stream pressure was set at 0.5 atmospheres. The free stream temperature was the same as in the previous case. In addition, the free stream flow was changed to be composed of stoichio-

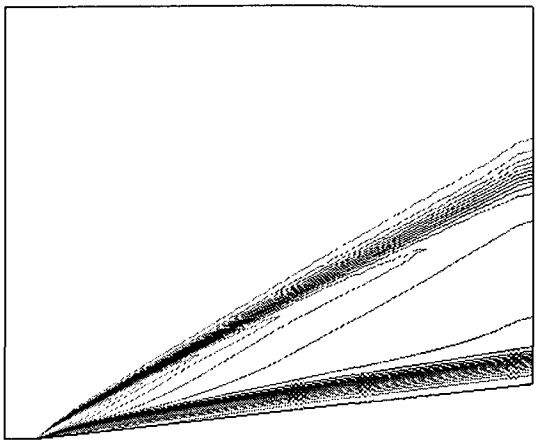

Figure 2: Density contours: $M = 2.92$ hydrogen/air 6.34° viscous ramp. Contour levels in kg/m^3: min: 0.011, max: 0.022, inc: 0.0007.

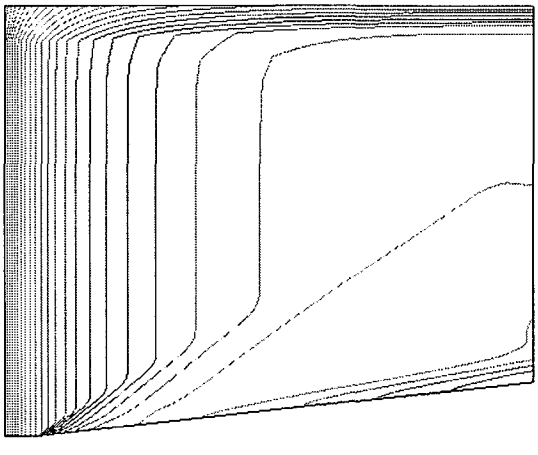

Figure 3: Logarithm of OH mass fraction contours: $M = 2.92$ hydrogen/air 6.34° viscous ramp. Contour levels: min: -3.57, max: -2.54, inc: 0.057.

metric hydrogen/air. This condition, as determined by Fielding [2], should be sufficient to cause strong reaction at least in the boundary layer. Temperature contours are depicted in Figure 4. The computed

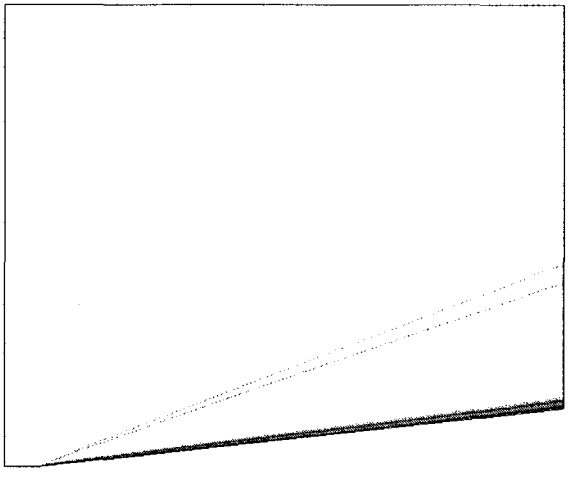

Figure 4: Temperature contours: $M = 4.00$ hydrogen/air 6.34° viscous ramp. Contour levels in K: min: 440, max: 2040, inc: 64.

shock angle is 18.7° while the exact solution gives a shock angle of 19.0°. The close agreement in this case is because the stoichiometric hydrogen/air flow does not react before passing through the shock, so that the Mach number in the inviscid free stream is then constant until the shock. In this flow, the increased pressure and temperature do indeed cause a noticeable reaction to occur in the boundary layer as shown by contours of water vapor mass fraction in Figure 5. The maximum mass fraction of water at this condition is approximately 16%.

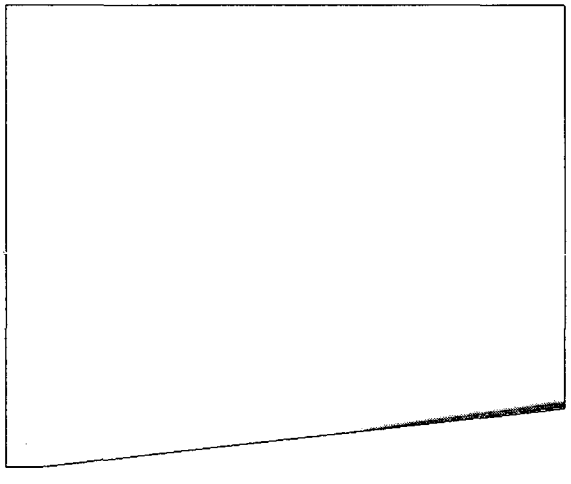

Figure 5: Water mass fraction contours: $M = 4.00$ hydrogen/air 6.34° viscous ramp. Contour levels: min: 0.0, max: 0.16, inc: 0.0073.

In this regime of flow conditions, the local Damköhler number in the boundary layer is sufficiently large to cause strong reactivity and transformation of reactants into products. However, strong exothermicity is not present, and the product forming region does not have enough time to grow out of the boundary layer through either species diffusion or heat transfer into the main flow. Thus, in order to achieve strong heat release and water vapor formation outside of the boundary layer at the length scale dictated by the size of the experimental apparatus, the free stream Mach number and pressure must be increased appreciably from their current levels. Alternatively, if the wind tunnel conditions remain fixed, a longer distance must be allowed for the reactions to develop so that the flow in the boundary layer has sufficient residence time to achieve stronger exothermicity.

The parallel speedup on an IBM SP-2 for the simulation of the reactive $M = 2.92$ hydrogen–air wedge flow is depicted in Figure 6. The additional work due to the chemical source terms and species diffusion effects increases the computational work per cell relative to an inviscid nonreacting simulation without increasing communication costs. This effect yields high parallel speedups even for a relatively coarse 64×48 mesh on large numbers of processors (more than 8). The high parallel speedups obtained for this chemical model will be sustained or increased for larger chemical models such as those necessary for hydrocarbons.

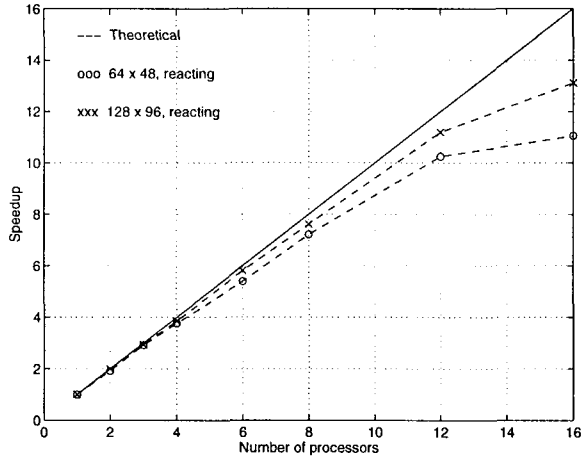

Figure 6: Parallel speedup for reactive $M = 2.92$ viscous wedge hydrogen/air case.

Two-dimensional methane/air combustion cases were computed using the mechanism of Yungster and Rabinowitz [23] which includes 19 reacting species and 52 reactions. One group of inviscid test cases consists of cylinders placed in an oncoming flow of stoichiometric methane/air. The cylinder diameters were 1 mm and 3 mm. The free stream temperature of the flow was 295 K, free stream pressure was 51600 Pa and the Mach number was 6.61. The flow around both cylinders was calculated first on a grid of size 64×72 and then on a grid of size 96×120 in order to achieve a grid–converged solution. The finer grid was constructed so that the grid spacing normal to the body was half the size as that of the coarser grid.

The first cylinder diameter was 1 mm. The oncoming flow forms a bow shock upstream of the cylinder which causes the temperature behind the shock to be about 2200 K with a pressure of 2.75 MPa. Under these conditions, the reactant species begin to break down, in small quantities, to form various radical species. Eventually, when sufficient amounts of radicals have built up, products are formed and heat is released, which causes further break down of reactants and product formation. The temperature along the stagnation streamline for both grids is depicted in Figure 7. As expected, the temperature

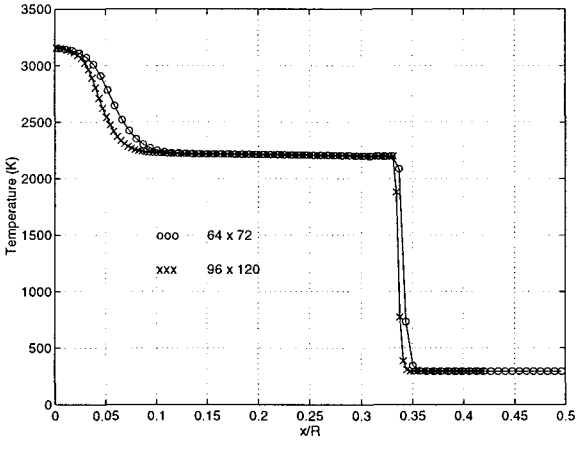

Figure 7: Temperature along stagnation streamline for two different size grids: $M = 6.61$ methane/air, 1 mm diameter, projectile surface at x/R = 0.00. Grid sizes: 64×72 and 96×120.

is approximately constant in the induction zone between the shock and the heat release region. Temperature contours for this case are shown in Figure 8. The varying strength of the shock causes the induction zone to vary in length. Eventually, at the outer regions of the flow domain, the shock is not strong enough to allow sufficient amounts of radicals to form to cause heat release. Density and pressure contours are shown in Figures 9 and 10. The results for the 1 mm diameter cylinder are in good agreement with those of Yungster and Rabinowitz [23]. The shock position predicted from Figure 7 is x/R = 0.34 while the result of Yungster and Rabinowitz gives a shock position of x/R = 0.37, a difference of 8.8%. The location of the initial heat release is predicted to be at x/R = 0.07; Yungster and Rabinowitz predict this point to be at x/R = 0.10. The

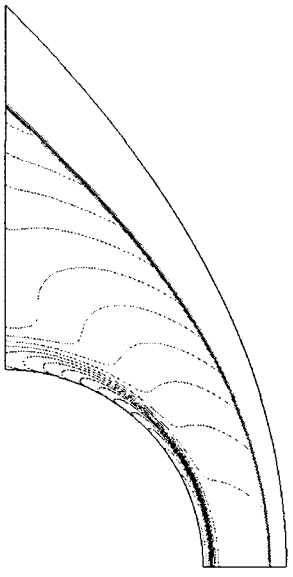

Figure 8: Temperature contours: $M = 6.61$ methane/air, 1 mm diameter. Grid size: 96×120.

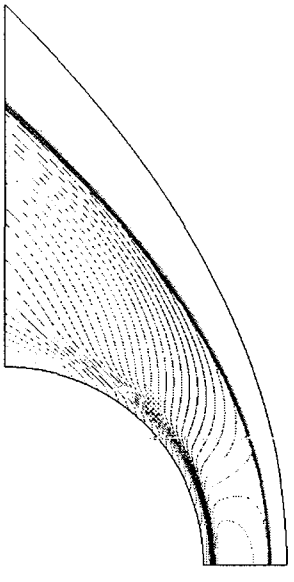

Figure 9: Density contours: $M = 6.61$ methane/air, 1 mm diameter. Grid size: 96×120.

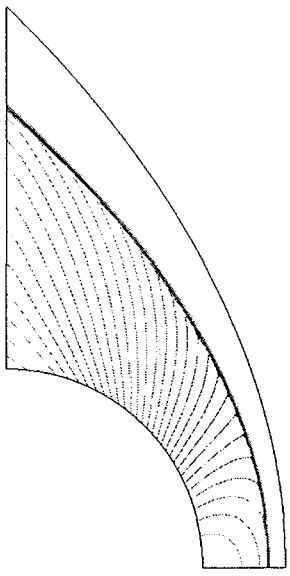

Figure 10: Pressure contours: $M = 6.61$ methane/air, 1 mm diameter. Grid size: 96×120.

chemistry results are fairly similar; for the 1 mm diameter body, Yungster and Rabinowitz predict a temperature at the stagnation point on the surface of the body of approximately 3100 K while the current simulation predicts a temperature of 3150 K.

Flow at $M = 6.61$ over a 3 mm diameter cylinder was also simulated. A graph of temperature along the stagnation streamline for both grids is presented in Figure 11. The nearly identical results for the two grids indicate that the solution is in fact grid converged. Temperature contours on the 96×120

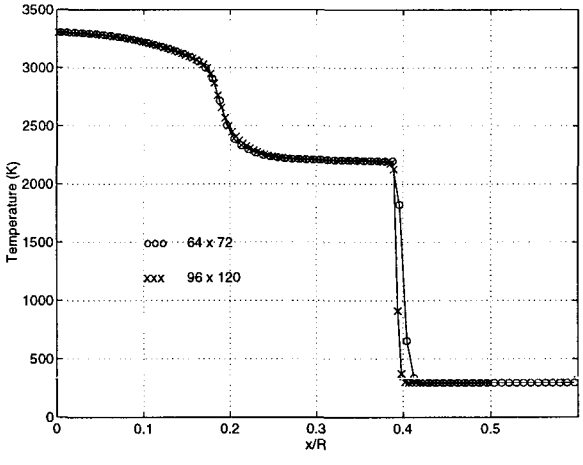

Figure 11: Temperature along stagnation streamline for two different size grids: $M = 6.61$ methane/air, 3 mm diameter, projectile surface at x/R = 0.00. Grid sizes: 64×72 and 96×120.

grid are presented in Figure 12 while density and pressure contours are shown in Figures 13 and 14. These results again show good agreement with the

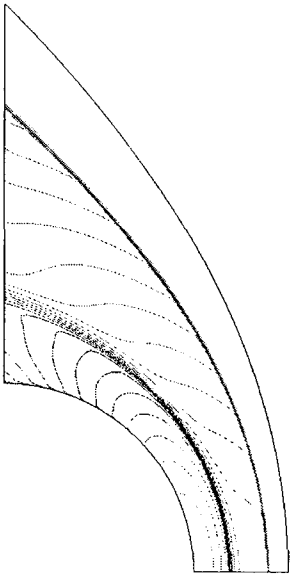

Figure 12: Temperature contours: $M = 6.61$ methane/air, 3 mm diameter. Grid size: 96×120.

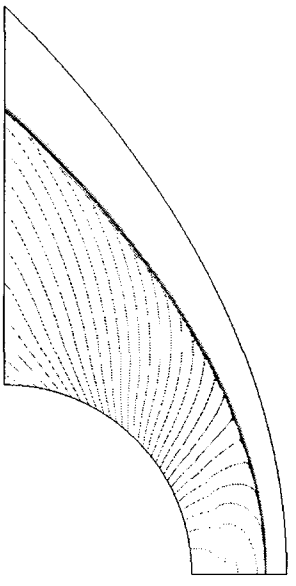

Figure 14: Pressure contours: $M = 6.61$ methane/air, 3 mm diameter. Grid size: 96×120.

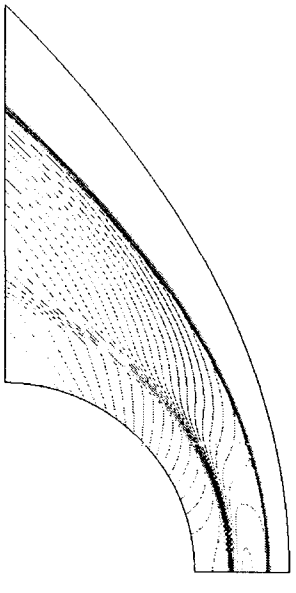

Figure 13: Density contours: $M = 6.61$ methane/air, 3 mm diameter. Grid size: 96×120.

work of Yungster and Rabinowitz. In this case, Figure 11 shows a shock location of x/R = 0.4 while the simulation of Yungster and Rabinowitz yields a shock location of approximately x/R = 0.46, a difference of 13%. The location of heat release is at x/R = 0.21 while a location of x/R = 0.32 is predicted by Yungster and Rabinowitz. Yungster and Rabinowitz predict a surface temperature of 3300 K and the current simulation predicts a temperature of 3300 K as well. Thus, the results of the chemistry are in quite good quantitative agreement.

Figures 15 through 18 depict the mass fractions of the various species along the stagnation streamline for the 3 mm diameter cylinder. As would be expected, the mass fractions of the radicals increase past the shock while the mass fractions of reactants stay approximately constant. When enough radical species have been formed, some products are created, liberating heat, which causes more radicals to form. These radicals react with the reactants, depleting their supply greatly in the heat release region and liberating more heat as more products are formed. One can also notice in Figure 16 the production and destruction of intermediate radicals between the shock and the heat release region. Higher order hydrocarbons (Figure 18) are created in the induction zone due to combination of some radical species, but these hydrocarbons are rapidly destroyed through the heat release region.

In general, the CUSP scheme handles the large increases and decreases in radical species mass fraction very well. The mass fraction results compare very favorably with those of Yungster and Rabinowitz in a qualitative sense. Locations of radical growth, de-

cay and maxima relative to the position of the shock and heat release front are similar. More quantitative comparisons cannot be made due to the different shock and heat release locations.

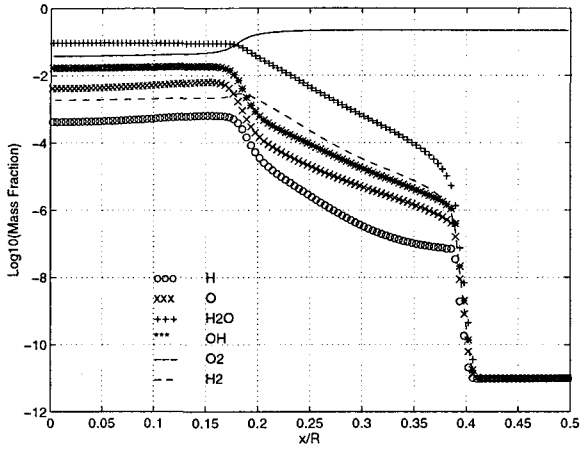

Figure 15: Species mass fractions along stagnation streamline: $M = 6.61$ methane/air, 3 mm diameter. Shock location is at x/R = 0.40, heat release begins at x/R = 0.21, projectile surface at x/R = 0.00. Grid size: 96 × 120.

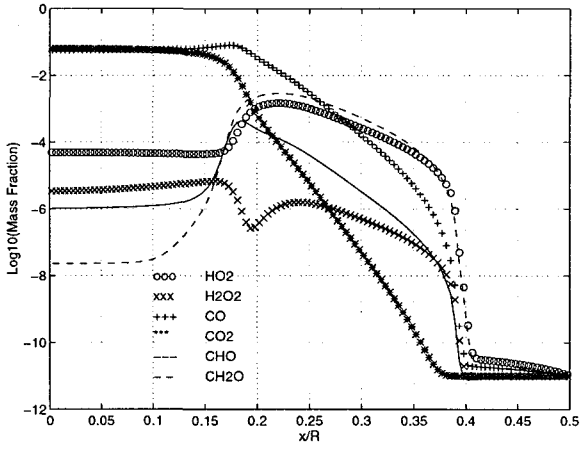

Figure 16: Species mass fractions along stagnation streamline: $M = 6.61$ methane/air, 3 mm diameter. Shock location is at x/R = 0.40, heat release begins at x/R = 0.21, projectile surface at x/R = 0.00. Grid size: 96 × 120.

A viscous laminar test case for hydrocarbon combustion consisted of a stoichiometric methane/air flow over a 10° ramp. The free stream Mach number was 4.0, the free stream temperature was 1200 K and the free stream pressure was one atmosphere. The 2 cm long ramp was preceded by a 1 cm solid wall section. The effects of viscosity, heat conduction and species diffusion are all included in this computation. This is a common diffusive/reactive test case for hydrogen/air flows. This simulation is intended

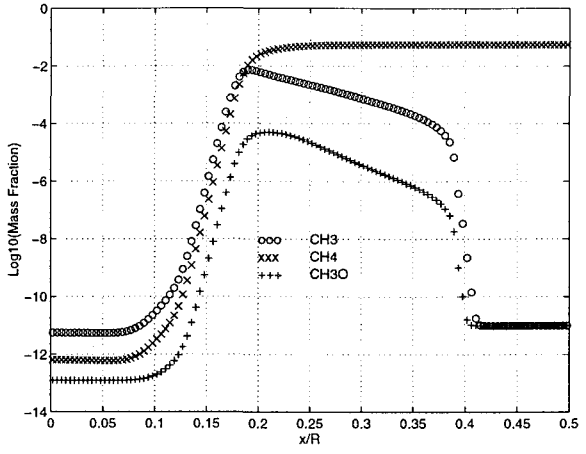

Figure 17: Species mass fractions along stagnation streamline: $M = 6.61$ methane/air, 3 mm diameter. Shock location is at x/R = 0.40, heat release begins at x/R = 0.21, projectile surface at x/R = 0.00. Grid size: 96 × 120.

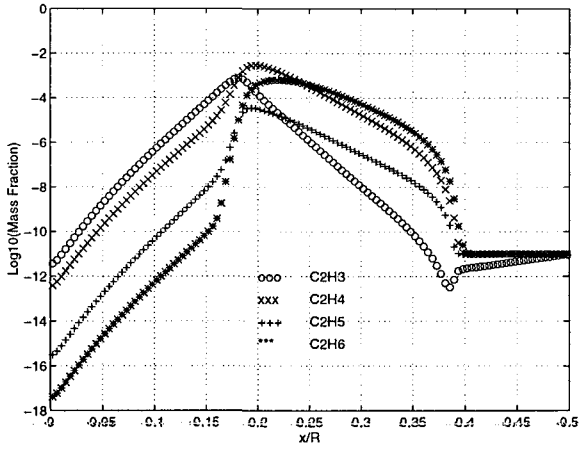

Figure 18: Species mass fractions along stagnation streamline: $M = 6.61$ methane/air, 3 mm diameter. Shock location is at x/R = 0.40, heat release begins at x/R = 0.21, projectile surface at x/R = 0.00. Grid size: 96 × 120.

to demonstrate the feasibility of calculations including both reactive and diffusive effects for hydrocarbons. The calculation was performed on a grid with 128 cells in the streamwise direction and 156 cells in the vertical direction. Approximately 32 cells were placed in the boundary layer to adequately capture the effects of diffusion near the wall. Temperature and density contours for this simulation are shown in Figures 19 and 20. A very weak oblique shock may

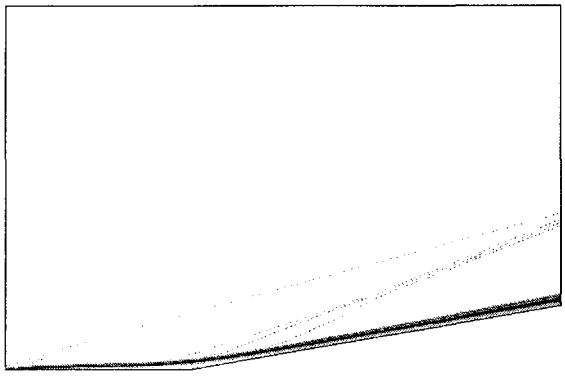

Figure 19: Temperature contours: $M = 4.00$ methane/air 10° viscous ramp, 128 × 156 grid.

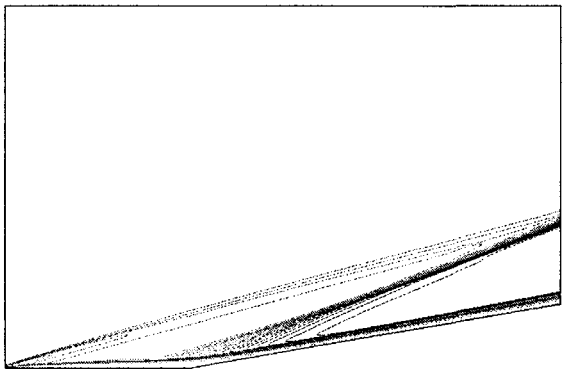

Figure 20: Density contours: $M = 4.00$ methane/air 10° viscous ramp, 128 × 156 grid.

be seen to emanate from the left edge of the wall due to the displacement thickness of the boundary layer. In addition, a recirculation region near the corner of the ramp is noted. The free stream temperature is not high enough to initiate a reaction, but the high temperature in the boundary layer and the pressure and temperature increase behind the oblique shock cause radicals to be created. Eventually, these radicals build up to sufficient levels to combine and form products such as carbon dioxide near the wall, as shown in Figure 21.

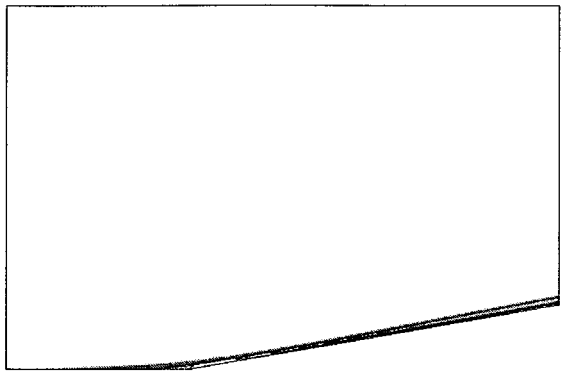

Figure 21: Carbon dioxide mass fraction contours: $M = 4.00$ methane/air 10° viscous ramp, 128 × 156 grid.

Conclusions

An accurate solver for the steady-state Euler and Navier-Stokes equations with chemical reactions has been developed and validated. The CUSP dissipation scheme yields accurate capture of shocks, reaction zones and reaction fronts for inviscid and viscous two-dimensional test cases while multigrid acceleration leads to a decrease in computational time without sacrificing accuracy. The point implicit treatment of the chemical source vector gives reasonable convergence rates using an explicit flow solver. In addition, the use of large chemical models for hydrocarbon combustion is facilitated by modest computational costs achieved through the use of multigrid and parallel programming.

Acknowledgements

This work was funded by AFOSR-URI F49620-93-1-0427. The first author was supported in part by a Fannie and John Hertz Foundation/Princeton Research Center Fellowship.

References

[1] T. R. A. Bussing and E. M. Murman. Finite–volume method for the calculation of compressible chemically reacting flows. *AIAA Journal*, 26(9):1070–1078, September 1988.

[2] J. Fielding. An experimental study of supersonic laminar reacting boundary layers. Master's thesis, Princeton University, Department of Mechanical and Aerospace Engineering, January 1997.

[3] M. Frenklach, H. Wang, and M. J. Rabinowitz. Optimization and analysis of large chemical kinetic mechanisms using the solution mapping method–combustion of methane. *Progress in Energy and Combustion Science*, 18:47–73, 1992.

[4] W. C. Gardiner, Jr., editor. *Combustion Chemistry.* Springer-Verlag, New York, 1984.

[5] A. Jameson. Analysis and design of numerical schemes for gas dynamics 1, artificial diffusion, upwind biasing, limiters and their effect on multigrid convergence. *Int. J. of Comp. Fluid Dyn.*, 4:171–218, 1995.

[6] A. Jameson. Analysis and design of numerical schemes for gas dynamics 2, artificial diffusion and discrete shock structure. *Int. J. of Comp. Fluid Dyn.*, 5:1–38, 1995.

[7] Y. Ju. Lower–upper scheme for chemically reacting flow with finite rate chemistry. *AIAA Journal*, 33(8):1418–14256, August 1995.

[8] R. J. Kee, G. Dixon-Lewis, J. Warnatz, M. E. Coltrin, and J. A. Miller. *A Fortran Computer Code Package for the Evaluation of Gas–Phase Multicomponent Transport Properties.* Sandia National Laboratories, Livermore, CA, May 1993. SAND 86-8246.

[9] T. J. Kim, R. A. Yetter, and F. L. Dryer. New results on moist CO oxidation: High pressure, high temperature experiments and comprehensive kinetic modeling. Twenty-Fifth Symposium (International) on Combustion, The Combustion Institute, 1994.

[10] L. Martinelli. *Calculation of Viscous Flows with a Multigrid Method.* PhD thesis, Princeton University, Department of Mechanical and Aerospace Engineering, October 1987.

[11] L. Martinelli and A. Jameson. Validation of a multigrid method for the Reynolds Averaged equations. *AIAA paper 88-0414*, AIAA 26th Aerospace Sciences Meeting, Reno, NV, January 1988.

[12] S. G. Sheffer. *Parallel Computation of Supersonic Reactive Flows with Detailed Chemistry Including Viscous and Species Diffusion Effects.* PhD thesis, Princeton University, Department of Mechanical and Aerospace Engineering, June 1997.

[13] S. G. Sheffer, A. Jameson, and L. Martinelli. A multigrid method for high speed reactive flows. *AIAA paper 97-2106*, AIAA 13th Computational Fluid Dynamics Conference, Snowmass Village, CO, June 29-July 2 1997.

[14] S. G. Sheffer, A. Jameson, and L. Martinelli. Parallel computation of supersonic reactive flows with detailed chemistry. *AIAA paper 97-0899*, AIAA 35th Aerospace Sciences Meeting, Reno, NV, January 6-9 1997.

[15] J. S. Shuen and S. Yoon. Numerical study of chemically reacting flows using a lower–upper symmetric successive overrelaxation scheme. *AIAA Journal*, 27(12):1752–1760, December 1989.

[16] S. Tatsumi, L. Martinelli, and A. Jameson. Design, implementation, and validation of flux limited schemes for the solution of the compressible Navier-Stokes equations. *AIAA paper 94-0647*, AIAA 32nd Aerospace Sciences Meeting, Reno, NV, January 1994.

[17] H. Wang and M. Frenklach. Detailed reduction of reaction mechanisms for flame modelling. *Combustion and Flame*, 87:365–370, 1991.

[18] F. A. Williams. *Combustion Theory.* Addison-Wesley Publishing Company, Reading, MA, 2nd edition, 1985.

[19] G. J. Wilson and R. W. MacCormack. Modeling supersonic combustion using a fully implicit numerical method. *AIAA Journal*, 30(4):1008–1015, April 1992.

[20] R. Yetter and J. Fielding. Princeton University, 1996. Private communication.

[21] R. A. Yetter, F. L. Dryer, and D. M. Golden. Pressure effects on the kinetics of high speed chemically reacting flows. ICASE/NASA Series, New York, 1992. Springer–Verlag. In Major Research Topics in Combustion.

[22] S. Yungster. Numerical study of shock–wave/boundary-layer interactions in premixed combustible gases. *AIAA Journal*, 30(10):2379–2387, 1992.

[23] S. Yungster and M. J. Rabinowitz. Computation of shock–induced combustion using a detailed methane–air mechanism. *Journal of Propulsion and Power*, 10(5):609–617, 1994.